Quantitative Photogrammetric Analysis of Digital Underwater Video Imagery

Rongxing Li, Haihao Li, Weihong Zou, Robert G. Smith, and Terry A. Curran

***Abstract*— This paper presents a photogrammetric model for digital underwater video imagery, which has been mostly applied to qualitative analysis in the marine environment. With this model, quantitative analysis of underwater images is possible, e.g., to locate positions, calculate sizes, and measure shapes of objects from image features. The underwater photogrammetric model is based on a three-dimensional optical ray tracing technique which rigorously models imaging systems with multilens configurations and multiple refractions. The calibration procedure with two independent phases has been proven to be efficient in simplifying the computation and improving the calibration accuracy. With the current imaging system configuration and photogrammetric model, an accuracy of 0.8 cm in lateral directions and 1.2 cm along the depth direction for objects located about 2–3 m from the camera system in the object space is attainable. A PC-based digital underwater photogrammetric prototype system has been developed to implement the underwater photogrammetric model.**

***Index Terms*— CCD image processing, underwater imaging, underwater photogrammetry, underwater vision.**

I. Introduction

VIDEO images have been mostly used in the underwater environment for qualitative analysis such as visualization of underwater archaeological sites, habit studies of sharks and other animals, and for behavior studies of water sports. In addition to these uses, however, there is a high demand for quantitative analysis of underwater images. This has been impossible in the past, or performed with a much reduced and limited capacity because of the lack of efficient tools, complete digital underwater photogrammetric models, and special softcopy underwater photogrammetric systems. Some examples are the size and shape measurement of fish species [1], [2], underwater equipment inspection and accurate motion monitoring [3], [4], and extremely large-scale seafloor mapping [5]–[7]. In comparison to acoustic imaging technology, which has dominated many areas of underwater imaging applications, underwater video images have the following advantages: 1) excellent image features which are essential for interpretation and measurement; 2) clear object projections in the images because of the optical imaging characteristics and relatively short distances between cameras and objects; and 3) high relative accuracy of measurements based on photogrammetric principles. In many applications, information contained in and derived from underwater video images is complementary to that of acoustic signals. For instance, micro features derived from the video images can be used to determine fish shapes and identify fish species [1].

This paper presents the results of collaborative research between the Department of Geomatics Engineering of The University of Calgary and the Canadian Hydrographic Services (CHS) of the Department of Fisheries and Oceans Canada. The objectives of the research were:

- to investigate optical imaging properties using charge coupled device (CCD) cameras in an underwater environment;
- to establish a photogrammetric model for *digital* underwater imaging systems in general and, in particular, the one developed by CHS;
- to design and implement a calibration procedure for routine applications of the system;
- to develop a software package for quantitative analysis of acquired images based on personal computers.

A discussion detailing the algorithms and the software system developed to meet the above objectives is presented in the following sections. System tests are included to show the performance of the imaging system when used for data acquisition and object measurement. The imaging system calibration procedure (through which positional and orientational parameters of cameras, media indexes of refraction, and cover lens parameters are calculated prior to operation) is also described. The accuracy of positional object measurements with the current configuration reaches 0.8 cm in lateral directions and 1.2 cm in the depth direction for objects located about 2–3 m from the camera system. Applications of this methodology may be found in situations where noncontact precision measurements are required.

II. Geometric Aspects of Underwater Imaging

A. Digital Underwater Photogrammetry

Underwater photogrammetry enables noncontact measurements of objects in the underwater environment. Through underwater photogrammetric models, three-dimensional (3-D) coordinates in the object space can be derived from the corresponding image coordinates measured.

Manuscript received August 7, 1995; revised June 6, 1996. This work was supported by the Natural Science and Engineering Research Council of Canada (NSERC), Canadian Hydrographic Services (CHS), and the Department of Fisheries and Oceans (DFO).

R. Li is with the Department of Civil and Environmental Engineering and Geodetic Science, The Ohio State University, Columbus, OH 43210 USA.

H. Li and W. Zou are with the Department of Geomatics Engineering, University of Calgary, Calgary, Alberta, T2N 1N4 Canada.

R. G. Smith and T. C. Curran are with Canadian Hydrographic Services, Sidney, BC, Canada.

Publisher Item Identifier S 0364-9059(97)01427-1.

Stereo photogrammetry has been successfully applied in land-based mapping and engineering projects [8], [9]. It requires that the camera exposure center, the image point, and the corresponding object point be on the same line (i.e., collinearity condition), so that photo triangulations can be used to determine positions of object points from different images. However, in the underwater environment, this collinear condition does not hold and standard photogrammetric triangulation cannot be applied directly. To overcome the difficulty, some "active" photogrammetric approaches have been implemented where signals such as laser beams [7] or grating patterns are actively projected on the object surfaces. Stereo models generated by the laser beams can be measured by using the hologrammetric principle [10]. Contour lines derived from the casted Moirè grating pattern provide direct depth information of the object [11], [6]. Some approaches require complicated procedures and accurate settings which would be mostly suitable for indoor situations and, thus, preclude the application in the underwater environment.

Early experiments of underwater analytical photogrammetry were reported by Pollio [12], [5] and Torlegard and Lundalv [13] on underwater mapping of the sea bottom, location, and mapping of shipwrecks, and measurements of marine biological specimens. Subsequently, for underwater safety inspection and maintenance, the oil and gas industry [14] demonstrated that photogrammetric techniques could generate measurements of the size and shape of an underwater object. This, in turn, has led to photogrammetry gaining acceptance as a means of producing reliable dimensional information in the underwater environment from images acquired by imaging systems operated by divers or mounted on manned or unmanned vehicles [15]–[18]. Underwater cameras are normally nonmetric and have to be calibrated either in a shallow-water tank [19] or on site in an underwater environment [3], [20]. The latter method is favored, because it has the advantage of including local variables so that the differences from one site to another can be taken into account. Refractive index changes in water which result from variations in density, salinity, pressure, and temperature cannot be controlled but can be photogrammetrically modeled [3], [15]. Specifically, Hoehle [21] and Okamoto [22] proposed a (3-D) optical ray tracing-based space-resection method to establish the analytical underwater photogrammetric model, which constitutes a starting point for the digital underwater photogrammetric model in this research.

Among others, the difficulties of underwater photogrammetric modeling are mainly due to: 1) uncertainty related to refraction at the multimedia interfaces and unknown changes in refractive index and 2) low image quality caused by poor underwater lighting and variations of absorption, scattering, and transparency of water. Although efforts were made to research analytical underwater photogrammetric models, they have not been practically applied because computers available had previously not been efficient enough to handle the complicated models, and the images had been in the analog form (mostly film or glass). The photogrammetric models developed were also dependent on specific imaging system configurations. In the late 1980's, the advance of digital image processing and computer hardware and software technologies greatly changed the thinking of photogrammetrists and led to the development of softcopy photogrammetric systems in which all operations are based on digital images [23], [24]. Despite the difficulties encountered, the extention of softcopy photogrammetric systems from land-based toward underwater applications has been increasingly researched [1], [25].

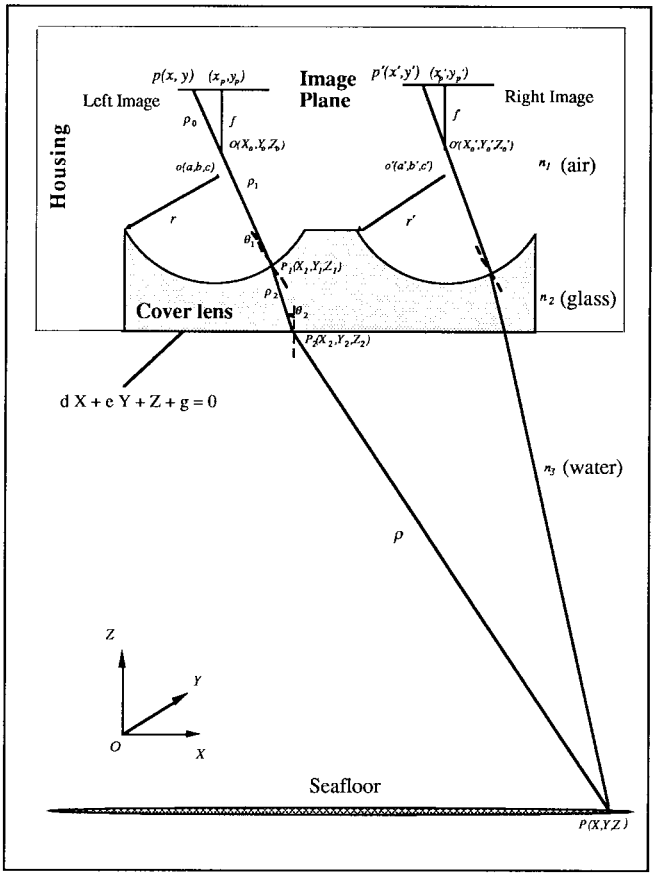

Fig. 1. Overview of the geometry of a typical underwater stereo imaging system showing geometry used for analysis described in the text.

B. The Imaging System

Geometrically, a typical underwater stereo imaging system has two major components, namely cameras and cover lenses, which affect paths of optical rays between photographed objects and their images (Fig. 1). The cover lenses are in the front of the cameras and are assembled on the cover of the housing that is waterproof and protects the system against high pressure when operated in a deep-water environment. The shape of the cover lenses could be convex or plane-concave (Fig. 1). Concave lenses increase the field of view and reduce distortion accordingly.

The following discussion is based on the left camera shown in Fig. 1. The results can be easily modified and applied to the right camera. On the image plane, the principal point, which is the intersection point between the image plane and the optical axis of the camera, has coordinates (x_p, y_p). The camera has a fixed focal length of f. Instead of a film, the CCD camera uses an array of pixels to detect and record the

reflected light intensity from objects in the illuminated field of view. The pixels are generally not perfectly square because of the irregularity of the pixel spacing in the x and y directions. A simplified way to compensate this effect is to define a scale change as a y-scale factor $s_y = dy/dx$ with dx and dy being pixel size in the x and y directions, respectively. CCD cameras are often of lower spatial resolution. Inaccuracies caused by, for example, linejitter occur. In addition, camera lens distortions δ_x and δ_y at the image point (x, y) in the x and y directions are modeled by the following equations [26]:

$$\begin{aligned}\delta_x &= K_1 x r^2 + K_2 x r^4 + Q_1(r^2 + 2x^2) + 2Q_2 xy \\ \delta_y &= K_1 y r^2 + K_2 y r^4 + Q_2(r^2 + 2y^2) + 2Q_1 xy \end{aligned} \quad (1)$$

with $r = (x^2 + y^2)^{1/2}$. The parameters of K_1 and K_2 model the symmetric lens distortion in the radial direction from the principal point caused mainly by the imperfection of the lens surface. Q_1 and Q_2 are parameters which model the decentering lens distortion at the image point in the direction tangential to the radial direction. The latter distortion is mainly caused by decentering of lens components of a complex lens along the optical axis.

Considering the ray traveling from the object point P to point p on the left image plane (Fig. 1), refractions take place because of the refractive index differences between media traveled. According to Snell's law in optics, refraction angles can be calculated if the media and the surface shapes of the cover lenses are known. Suppose that P_1 and P_2 are points where the optical ray refracts on the inner and outer surfaces of the cover. The ray P-$P_2(\rho)$ is refracted with an angle θ_2 at P_2. Ray P_2-$P_1(\rho_2)$ is further refracted with an angle of θ_1 at P_1. Finally, the projection of points (including P_1) on the concave surface of the cover lens onto the image plane obeys the perspective projection law.

There are no restrictions to relative positions and orientations of the cameras. The camera position is described by its exposure center O with coordinates (X_o, Y_o, Z_o), while its orientation is depicted by three rotation angles ω, ϕ, and κ, defined according to the object coordinate system (O-XYZ). The perspective projection gives a geometric relationship between the image coordinates (x, y) and coordinates (X_1, Y_1, Z_1) of the corresponding point on the concave surface of the cover lens [8]:

$$\begin{aligned} x - x_p + \delta_x &= -f\frac{m_{11}(X_1 - X_o) + m_{12}(Y_1 - Y_o) + m_{13}(Z_1 - Z_o)}{m_{31}(X_1 - X_o) + m_{32}(Y_1 - Y_o) + m_{33}(Z_1 - Z_o)} \\ y - y_p + \delta_y &= -f\frac{m_{21}(X_1 - X_o) + m_{22}(Y_1 - Y_o) + m_{23}(Z_1 - Z_o)}{m_{31}(X_1 - X_o) + m_{32}(Y_1 - Y_o) + m_{33}(Z_1 - Z_o)} \end{aligned} \quad (2)$$

where m_{ij} ($i = 1, 2, 3$ and $j = 1, 2, 3$) are elements of a rotation matrix M and functions of the sines and cosines of orientation angles ω, ϕ, and κ. Since the concave surface of the cover lens can be treated as a sphere with a radius r and a center $o(a, b, c)$, a condition is added to (2):

$$(X_1 - a)^2 + (Y_1 - b)^2 + (Z_1 - c)^2 = r^2. \quad (3)$$

The front surface of the cover is flat and modeled using a (3-D) plane equation:

$$dX + eY + Z + g = 0 \quad (4)$$

with d, e, and g being the plane parameters. Because both surfaces are modeled without any restrictions, there are no constraints imposed on the location and orientation of the cover lenses for manufacturing.

III. Calculation of Coordinates in the Object Space by Ray Tracing

An important objective in many applications is the calculation of coordinates of points in the object space from measured corresponding points in the resulting stereo images. This is realized by tracing the rays starting from two corresponding image points p and p' (Fig. 1). The rays travel through different media and change the direction of their paths due to refraction and, finally, intersect at the object point P. The following sections describe the ray tracing procedure and the methodology by which the coordinates of P can be determined.

A. A General Refraction Model

Within an imaging system, the optical path of a light ray originating from an arbitrary selected point in the object space with a given starting propagation direction can be traced by Fermat's principle or by the successive use of Snell's law in uniform refractive index media having abrupt discontinuities. Algebraic and trigonometric expressions governing the precise path of a chosen initial ray can be derived as ray tracing equations. From these equations, the exact intersecting ray on the image plane or indeed on any chosen image surface can be determined.

In Fig. 2, a light ray originating at a point $P_0(X_0, Y_0, Z_0)$ propagates to $P_{p+1}(X_{p+1}, Y_{p+1}, Z_{p+1})$ through p refractive surfaces, which separate $p + 1$ different homogenous media with refractive indexes $n_i\,(i = 1, 2, \cdots, p + 1)$. The length of the ray segment between the $(i - 1)$th and ith surface is represented as an auxiliary quantity

$$\rho = \sqrt{(X_i - X_{i-1})^2 + (Y_i - Y_{i-1})^2 + (Z_i - Z_{i-1})^2}. \quad (5)$$

Generally, a light ray between P_0 and P_{p+1} will be refracted at every refractive surface discontinuity (interface). In this case, it is assumed that the coordinates of P_0 and P_{p+1} are known as well as the refractive surfaces by their implicit functions

$$F_i(X_i, Y_i, Z_i) = 0, \qquad i = 1, 2, \cdots, p. \quad (6)$$

Furthermore, we assume that derivatives

$$\left[\left(\frac{\partial F_i}{\partial X_i}\right)_{p_i}, \left(\frac{\partial F_i}{\partial Y_i}\right)_{p_i}, \left(\frac{\partial F_i}{\partial Z_i}\right)_{p_i}\right]^T$$

at the intersection point P_i exist. At each refractive point P_i, Snell's law is applied:

$$n_i \sin\theta_i = n_{i+1} \sin\theta_i'. \quad (7)$$

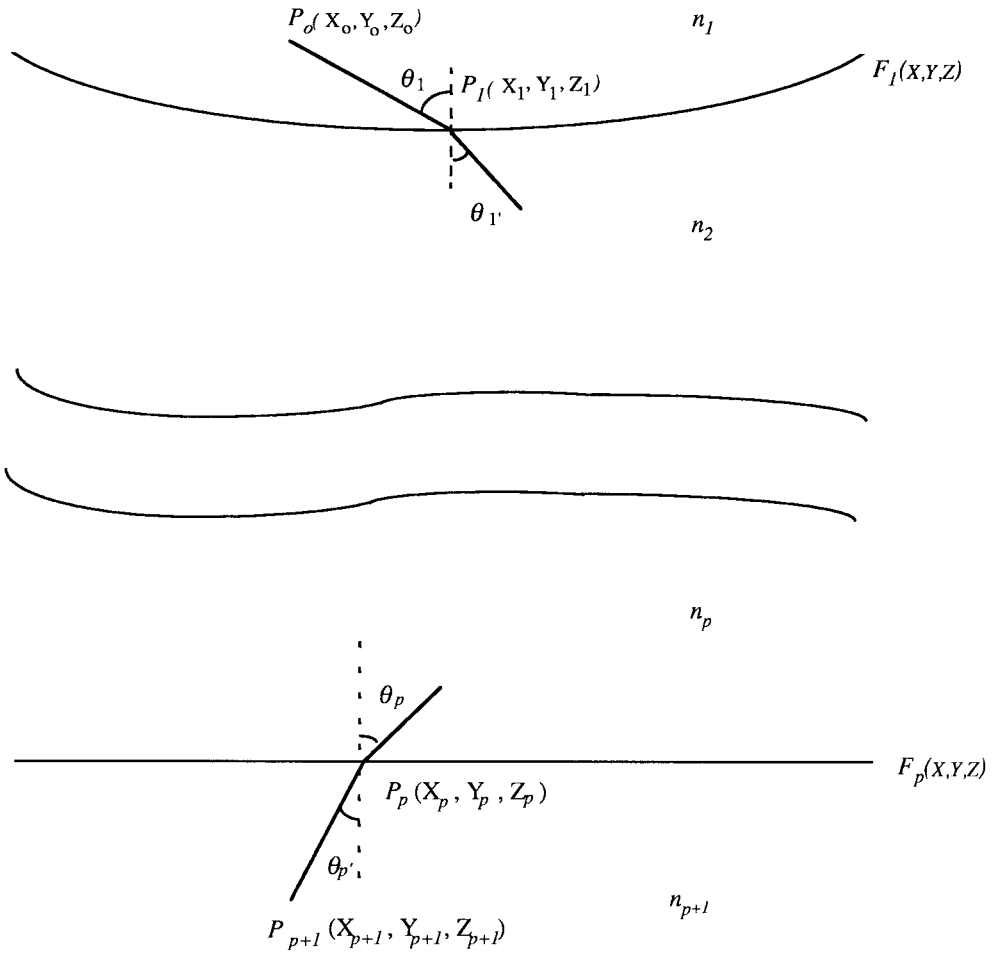

Fig. 2. Detail of ray tracing through p refractive surfaces [see (5)–(12)].

In order to trace the ray, it is necessary to find θ_i and θ_i' defined according to the incident ray, the normal of the surface, and the refracted ray. For θ_i, it can be obtained from

$$\cos\theta_i = \alpha_i\lambda_i + \beta_i\mu_i + \gamma_i\nu_i \tag{8}$$

where α_i, β_i, and γ_i are direction cosines of the ray from P_{i-1} to P_i, and λ_i, μ_i, and ν_i are elements of the normal vector of the refractive surface F_i at point P_i. α_i, β_i, and γ_i can be derived from

$$\begin{pmatrix}\alpha_i\\ \beta_i\\ \gamma_i\end{pmatrix} = \frac{1}{\rho_i}\begin{pmatrix}X_i - X_{i-1}\\ Y_i - Y_{i-1}\\ Z_i - Z_{i-1}\end{pmatrix} \tag{9}$$

and λ_i, μ_i, and ν_i can be expressed by

$$\begin{pmatrix}\lambda_i\\ \mu_i\\ \nu_i\end{pmatrix} = \left[\left(\frac{\partial F_i}{\partial X_i}\right)_{p_i}^2 + \left(\frac{\partial F_i}{\partial Y_i}\right)_{p_i}^2 + \left(\frac{\partial F_i}{\partial Z_i}\right)_{p_i}^2\right]^{-\frac{1}{2}} \begin{pmatrix}\left(\frac{\partial F_i}{\partial X_i}\right)_{p_i}\\ \left(\frac{\partial F_i}{\partial Y_i}\right)_{p_i}\\ \left(\frac{\partial F_i}{\partial Z_i}\right)_{p_i}\end{pmatrix}. \tag{10}$$

Similar to (8), θ_i' can be obtained so that

$$\cos\theta_i' = \alpha_{i+1}\lambda_i + \beta_{i+1}\mu_i + \gamma_{i+1}\nu_i \tag{11}$$

where α_{i+1}, β_{i+1}, and γ_{i+1} are direction cosines of the refracted ray or the incident ray referring to the $(i+1)$th refractive surface.

Using (7), (8), and (11), and given that the incident ray and the normal and the refracted ray lie on the same plane, it can be shown that

$$\begin{pmatrix}\alpha_{i+1}\\ \beta_{i+1}\\ \gamma_{i+1}\end{pmatrix} = \frac{n_i}{n_{i+1}}\begin{pmatrix}\alpha_i\\ \beta_i\\ \gamma_i\end{pmatrix} - \left(\frac{n_i}{n_{i+1}}\cos\theta_i - \cos\theta_i'\right)\begin{pmatrix}\lambda_i\\ \mu_i\\ \nu_i\end{pmatrix}. \tag{12}$$

Thus, the refracted ray can be calculated if the direction cosines of the incident ray and the normal and the refractive indexes are known.

B. The Underwater Photogrammetric Model

Considering the special configuration of Fig. 1, an underwater photogrammetric model can be developed to determine (X, Y, Z) of the point P in the object space based on the measured coordinates (x, y) and (x', y') of points p and

p' in the left and right image plane, respectively, under the assumption that the following 41 parameters are known:

- eight interior camera orientation parameters for locations of the principal points (x_p, y_p, x'_p, y'_p), the focal lengths (f, f'), and the y-scale factors (s_y, s'_y);
- eight polynomial coefficients for radial and decentering lens distortion corrections $(K_1, K_2, Q_1, Q_2, K'_1, K'_2, Q'_1, Q'_2)$;
- twelve exterior camera orientation parameters for locations and rotations of the camera exposure stations $(X_o, Y_o, Z_o, \omega, \phi, \kappa, X'_o, Y'_o, Z'_o, \omega', \phi', \kappa')$;
- eleven multilens parameters for the spatial definition of the cover lens surfaces $(a, b, c, r, a', b', c', r', d, e, g)$; and
- two parameters for refractive indexes of the cover lens and water (n_2, n_3).

The primed parameters above are related to the right image. Examining the left ray from p to P, the direction of the starting segment ρ_o from p to O can be expressed as [1]

$$\begin{pmatrix}\alpha_1\\ \beta_1\\ \gamma_1\end{pmatrix} = \frac{1}{\rho_o} M \begin{pmatrix} x\\ y\\ -f\end{pmatrix} \tag{13}$$

where ρ_o is equal to $(x^2+y^2+f^2)^{1/2}$ and M is the rotation matrix from the image coordinate system to the object space coordinate system used in (2).

The segment ρ_1 from O to P_1 is the extension of ρ_o and shares the same direction $(\alpha_1, \beta_1, \gamma_1)^T$. Its length can be calculated, with consideration of (3) and (5), as

$$\begin{aligned}\rho_1 = &-[\alpha_1(X_o-a)+\beta_1(Y_o-b)+\gamma_1(Z_o-c)]\\ &+\{[\alpha_1(X_o-a)+\beta_1(Y_o-b)+\gamma_1(Z_o-c)]^2\\ &-[(X_o-a)^2+(Y_o-b)^2+(Z_o-c)^2-r^2]\}^{\frac{1}{2}}.\end{aligned} \tag{14}$$

Furthermore, the coordinates of P_1 are

$$\begin{pmatrix}X_1\\ Y_1\\ Z_1\end{pmatrix} = \rho_1 \begin{pmatrix}\alpha_1\\ \beta_1\\ \gamma_1\end{pmatrix} + \begin{pmatrix}X_o\\ Y_o\\ Z_o\end{pmatrix}. \tag{15}$$

Cosines $(\lambda_1, \mu_1, \upsilon_1)^T$ of the normal of the spherical surface at point P_1 are obtained using (3) and (10):

$$(\lambda_1, \mu_1, \nu_1)^T = \left(\frac{X_1-a}{r}, \frac{Y_1-b}{r}, \frac{Z_1-c}{r}\right)^T. \tag{16}$$

From (12), the change in direction due to the refraction by the cover lens (spherical surface) is expressed as (17), shown at the bottom of the page, with $\cos\theta_1 = \alpha_1\lambda_1 + \beta_1\mu_1 + \gamma_1\nu_1$.

The refracted ray segment ρ_2 within the cover lens has a length of

$$\rho_2 = \frac{dX_1 + eY_1 + Z_1 + g}{d\alpha_2 + e\beta_2 + \gamma_2} \tag{18}$$

which is derived similarly as (14). Subsequently, the coordinates of P_2 can be obtained as

$$\begin{pmatrix}X_2\\ Y_2\\ Z_2\end{pmatrix} = \rho_2 \begin{pmatrix}\alpha_2\\ \beta_2\\ \gamma_2\end{pmatrix} + \begin{pmatrix}X_1\\ Y_1\\ Z_1\end{pmatrix}. \tag{19}$$

Cosines $(\lambda_2, \mu_2, \upsilon_2)^T$ of the normal of the planar surface at point P_2 are obtained using (4) and (10):

$$(\lambda_2, \mu_2, \nu_2)^T = \frac{1}{(d^2+e^2+1)^{1/2}}(d, e, 1)^T. \tag{20}$$

By similar development to (17), the change in direction due to the refraction by the cover lens on the planar surface is expressed as (21), shown at the bottom of the page, where n_3 is the refractive index of water and $\cos\theta_2 = \alpha_2\lambda_2 + \beta_2\mu_2 + \gamma_2\nu_2$.

With known coordinates $(X_2, Y_2, Z_2)^T$ of point P_2 and the direction $(\alpha_3, \beta_3, \gamma_3)^T$ of the ray segment ρ from P_2 to P, the coordinates of the object point P can be expressed as

$$\begin{pmatrix}X\\ Y\\ Z\end{pmatrix} = \rho \begin{pmatrix}\alpha_3\\ \beta_3\\ \gamma_3\end{pmatrix} + \begin{pmatrix}X_2\\ Y_2\\ Z_2\end{pmatrix}. \tag{22}$$

In (22), the four unknowns are the length of the ray segment ρ and the coordinates $(X, Y, Z)^T$. Rearranging for the elimination of ρ, (22) becomes

$$\begin{aligned}\gamma_3 X - \alpha_3 Z - \gamma_3 X_2 + \alpha_3 Z_2 = 0\\ \gamma_3 Y - \beta_3 Z - \gamma_3 Y_2 + \beta_3 Z_2 = 0.\end{aligned} \tag{23}$$

Equation (23) requires additional information to solve for the coordinates $(X, Y, Z)^T$. This can be obtained by considering that a corresponding light ray from the right image point p' will give an intersection at point P (Fig. 1). Analogous to

$$\begin{pmatrix}\alpha_2\\ \beta_2\\ \gamma_2\end{pmatrix} = \frac{n_1}{n_2}\begin{pmatrix}\alpha_1\\ \beta_1\\ \gamma_1\end{pmatrix} - \left[\frac{n_1}{n_2}\cos\theta_1 - \sqrt{1-\left(\frac{n_1}{n_2}\right)^2+\left(\frac{n_1}{n_2}\cos\theta_1\right)^2}\right]\begin{pmatrix}\lambda_1\\ \mu_1\\ \nu_1\end{pmatrix} \tag{17}$$

$$\begin{pmatrix}\alpha_3\\ \beta_3\\ \gamma_3\end{pmatrix} = \frac{n_2}{n_3}\begin{pmatrix}\alpha_2\\ \beta_2\\ \gamma_2\end{pmatrix} - \left[\frac{n_2}{n_3}\cos\theta_2 - \sqrt{1-\left(\frac{n_2}{n_3}\right)^2+\left(\frac{n_2}{n_3}\cos\theta_2\right)^2}\right]\begin{pmatrix}\lambda_2\\ \mu_2\\ \nu_2\end{pmatrix} \tag{21}$$

(23), the following equations describe the right intersecting ray:

$$\gamma_3' X - \alpha_3' Z - \gamma_3' X_2' + \alpha_3' Z_2' = 0$$
$$\gamma_3' Y - \beta_3' Z - \gamma_3' Y_2' + \beta_3' Z_2' = 0. \quad (24)$$

A least squares solution using (23) and (24) will give an estimate of the unknowns (X, Y, Z).

IV. Imaging System Calibration

In order to calculate 3-D coordinates in object space from measured corresponding image coordinates through the photogrammetric model based on (23) and (24), all unknown parameters need to be determined *a priori*. These include eight interior parameters, twelve exterior parameters, eight polynomial coefficients of lens distortion, eleven multilens parameters, and two refractive indexes. These 41 unknown parameters are defined in (1)–(24). The procedure for determining these parameters is called photogrammetric calibration.

Calibration of an imaging system is not a straightforward calculation problem. It is closely dependent on the physical configuration of the system. For instance, through the calibration, the relative positional and orientational relationships between two cameras in the housing are calculated using the data available at the time of calibration. The parameters will, however, be applied to the same cameras at a later time during the data acquisition for the geometric intersection and analysis. This requires that the relative positional and orientational changes between the two cameras during the period should be so small that the effect, thus caused, can be neglected. Similarly, the cover lenses are also not allowed to have any significant displacement after the calibration. In general, a recalibration is occasionally necessary, say once a month, or whenever a change of the system configuration, which affects the calibration parameters, is suspected. Sometimes, to compensate the refractive index change caused by different water bodies, on-site calibrations at sea are appropriate.

For the required calibration in this research, a set of control points (also called reference points) with known 3-D coordinates in the object space should be established. The image coordinates of the corresponding control points in the image pair can be measured. If a sufficient number of control points are available, the unknown parameters can be solved through linearized equations (1)–(24) using the least squares principle [1]. However, considering the complexity of the equations after the linearization with so many unknowns and possible correlations between them, the calibration procedure is separated to two phases in order to avoid potential computational problems and to simplify the calibration procedure. In phase one, the CCD cameras are calibrated where a pair of images with control points are determined in air without cover lenses. A traditional photogrammetric space resection can be employed to solve for the interior and exterior parameters (x_p, y_p, f, X_o, Y_o, Z_o, ω, ϕ, and κ for both cameras), camera lens distortion correction parameters (K_1, K_2, Q_1, and Q_2 for both cameras), and y-scale factors (s_y, s_y'). Thus, the effects of underwater ray bending and lens distortion do not need to be considered. Furthermore, clearer and sharper images can be obtained, compared to images taken underwater. Based on the above discussion, more accurate calibration results are expected from the first phase of calibration. In the second phase of the calibration, parameters associated with multiple lenses and different media are estimated, including parameters for defining the curved and planar surfaces of the left and right cover lenses, and refractive indexes of water and glass, respectively. If the refractive indexes of water and glass can be predetermined with high accuracy, they can be excluded to reduce the calibration complexity. It is noted that in this two-phase calibration procedure the cover lenses are treated as refractive media rather than a part of the camera system components. The cover lens parameters are determined in the second phase using the ray tracing technique. The calibration phase two is realized by sealing the cover of the camera housing, with the relative positions and orientations of the cameras retained; the camera system is then submerged into a water tank (Fig. 3). In both calibration phases, images are taken in which control points can be identified and measured. With the measured image coordinates and known coordinates in the object space, parameters can be calculated by using the two sets of independent equations. A detailed description of the calibration algorithms is published in Li [1].

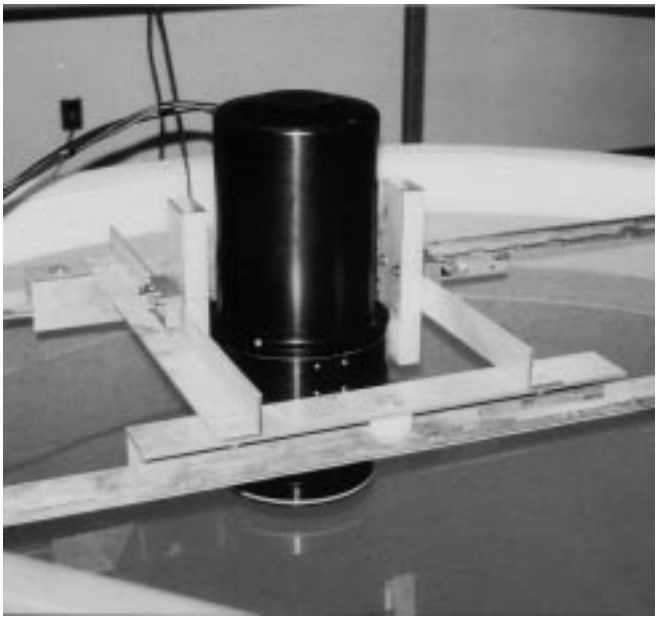

Fig. 3. Water tank test at the Canadian Hydrographic Services.

V. Implementation

A. A PC-Based Software System

To implement the underwater photogrammetric model and imaging system calibration model, a software system has been developed based on personal computers in the DOS environment. Fig. 4 illustrates modules implemented in this system. A highly object-oriented window toolkit WNDX (1992) is applied for developing the graphic user interface (GUI) of the system. Application modules developed in C and C++ programming language can be integrated with the WNDX GUI

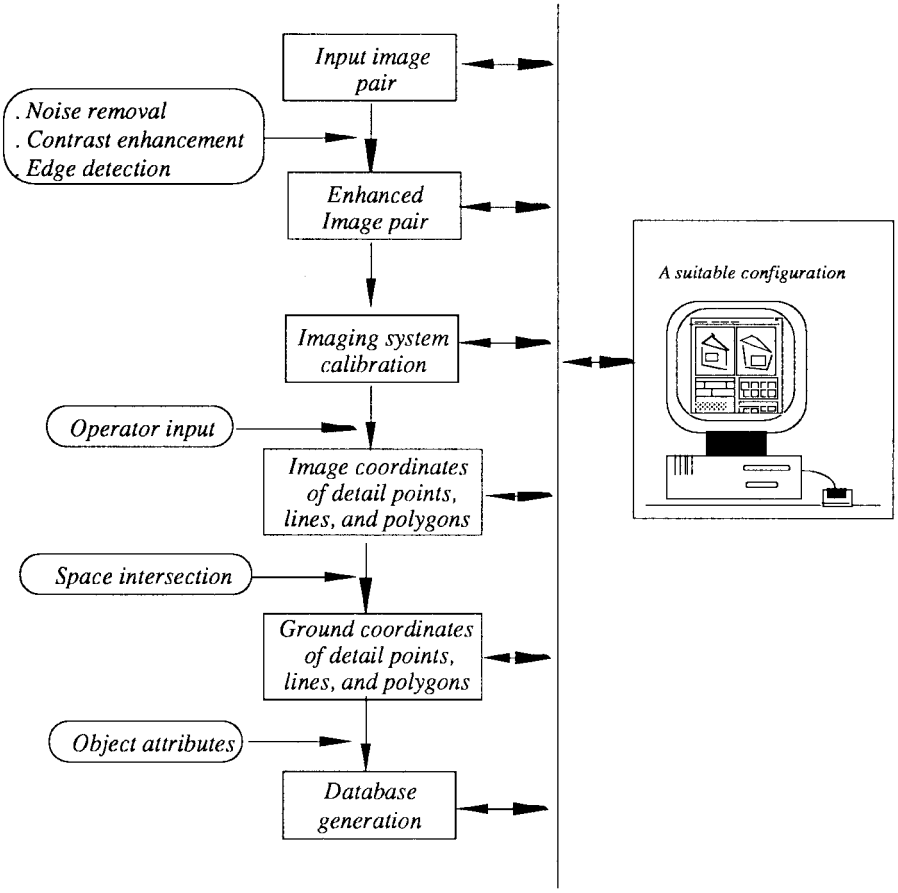

Fig. 4. Block diagram of software modules developed.

very easily. The software system is also transferable to most UNIX-based platforms.

The quality of underwater video images is usually poor in comparison to images taken in the open air-based environment, with main contributors being low and inhomogeneous visibility as well as image noise. This often makes it necessary to have the images preprocessed before use in photogrammetric processing (Fig. 4). The preprocessing operations include brightness adjustment, contrast enhancement, edge enhancement, and noise reduction.

If images to be processed were taken by a calibrated imaging system, the parameters in the photogrammetric model are available and the imaging system calibration module could be bypassed. Otherwise, a two-phase calibration must be performed. The software has been structured to require two independent steps.

1) With one image pair taken in air, conventional collinearity equations are used with an added polynomial being required to model lens distortions in order to perform the calibration adjustment. In this case, the interior parameters, such as focal length, principal points image scale, and lens distortion parameters, as well as exterior parameters, can be obtained.
2) Using the parameters derived from the first step, another image pair is taken underwater and the photogrammetric model developed by ray tracing is applied to calibrate the remaining unknowns. In this way, parameters specific to the geometry of the cover lens surfaces and the refractive indexes of water and the cover glass can be estimated.

The software system allows the operator to identify control targets and measure their image coordinates on the stereo image pair interactively (Fig. 5). Once a pair of conjugate image points are measured, the corresponding 3-D coordinates of the target stored in a control data file are associated. If a sufficient number of well-distributed control targets are selected, a reasonable calibration result can be expected.

Objects to be measured can be defined in terms of three geometric element types, namely points, lines, and polygons (Fig. 5). To complete an element, the operator digitizes the object on the stereo images accordingly. Using the photogrammetric model, the system makes space intersections in the object space from the conjugate image points and builds 3-D geometric elements with object space coordinates. Attribute information such as fish species and composition of the seafloor can be inferred by interpreting image features and associated geometric elements. After an object is measured, a record is made to describe its constituent geometric elements along with attributes, in order to generate spatial databases [27].

B. CCD Camera System I

Two Cosmicar brand CCD cameras with standard NTSC video signal output were major components of the underwater imaging system. Images produced by using PLL synchronized

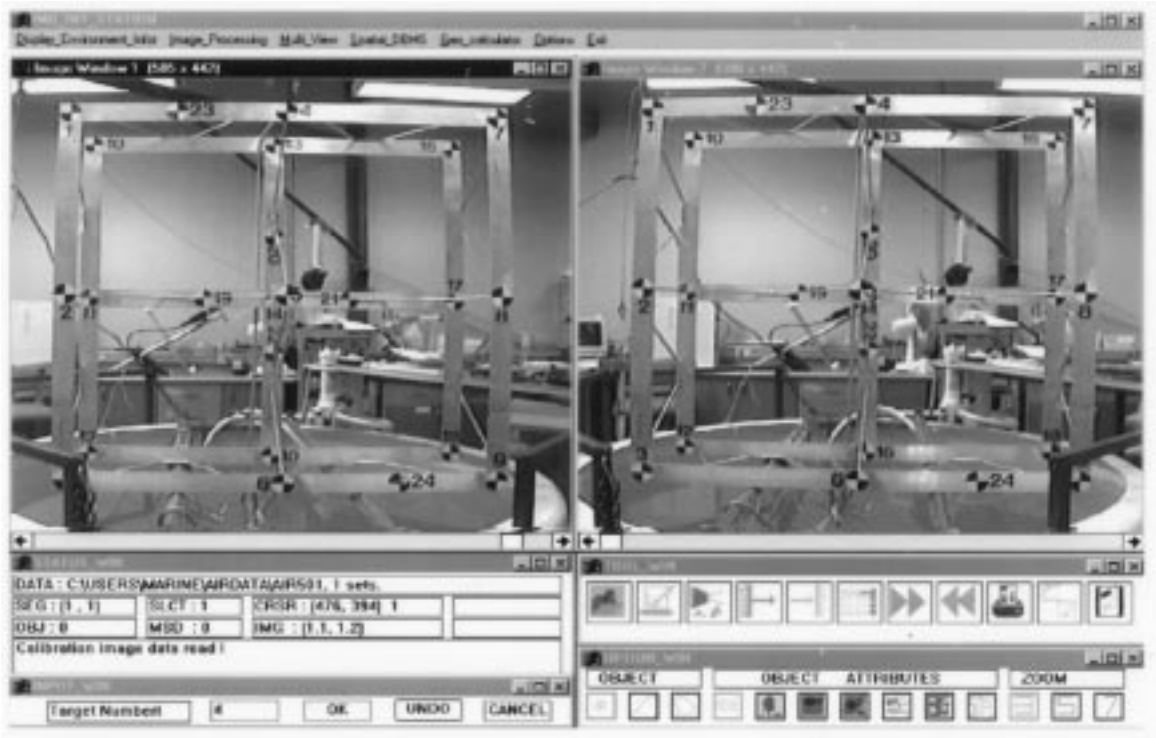

Fig. 5. Object measurement in the GUI environment of the software system.

frame grabbing have a size of 736 pixels by 488 pixels in the horizontal and vertical directions, respectively. They were fitted into a housing with a front cover containing two concave lenses which provide an enlarged field of view of 58° horizontal and 45° vertical. The housing is a waterproof and cylindrically shaped container (Fig. 3). To provide stereo vision, the two CCD cameras inside the housing were situated to maintain a fixed photobase of about 7 cm. The optical axes of the two cameras were parallel to within 1.5°. This ensured that each pair of images produced a usable stereo model with a more than 90% overlap area. Because the photogrammetric model is based on 3-D optical ray tracing, the cover lenses were considered. Thus, misalignment of the CCD cameras and corresponding cover lenses could be modeled using the photogrammetric model.

C. CCD Camera System II

This is an improved imaging system using two Sony ultrasmall interline CCD color cameras with an image size of 768×494 (pixels). The sensing area is 6.4 mm × 4.8 mm. To increase the camera baseline, a baseline bar is attached to a remotely operated vehicle (ROV) (see Fig. 6). The two cameras can move along the bar to form baselines of different lengths, with a maximum of about 0.4 m. The stereo overlap area can also be adjusted by changing the convergent angles of the cameras. This makes the concave surface of the cover lens in the imaging system I unnecessary. Each camera has its own housing with a flat glass cover plane. The ROV has a 3-D motion capability and is operable at down to 200 m under sea level. It is also equipped with an illuminating source using two halogen lamps (USHIO, Japan).

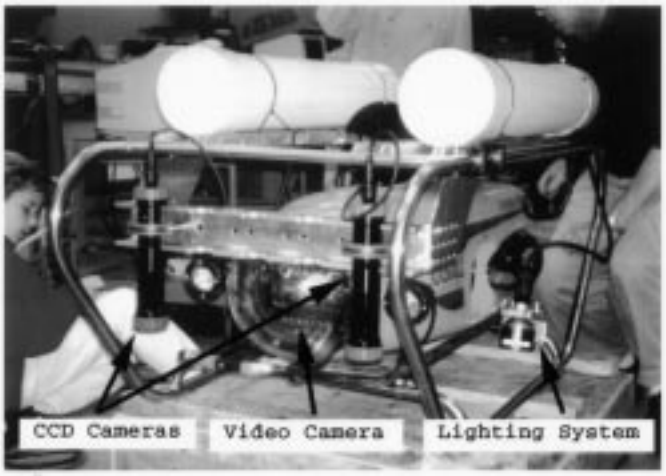

Fig. 6. CCD imaging system II.

D. Calibration Frame

In the calibration procedure, control targets with known coordinates in the object space are needed to calculate parameters in the photogrammetric model. Due to difficulties associated with underwater tests, the accuracy of the control points was suspect in our initial trials. The problem was resolved by introducing a portable and stable frame with well-defined targets which are well distributed three-dimensionally (Fig. 7). It is a 1.4 m × 1.4 m × 0.7 m rectangular aluminum frame with 24 control targets marked with highly reflective circular discs with an 8-cm diameter and a well-defined center. The coordinates of the targets in the object space are acquired by a precision micro survey that measures distances between targets

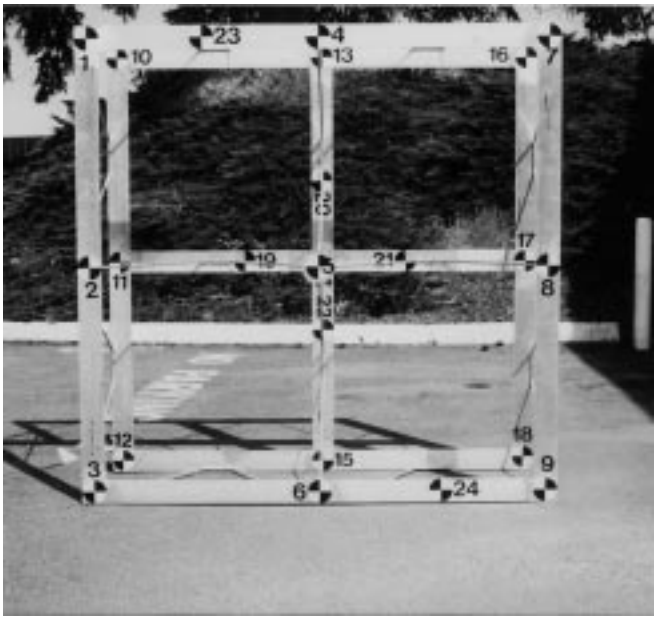

Fig. 7. The frame with control targets for imaging system calibration.

with all different combinations of target pairs using a precise engineering surveying tape. A least squares adjustment treats all the distances as observations and the 3-D coordinates of the targets are calculated by the COGO system [28]. The root mean square (rms) error of the target coordinates is 1 mm.

E. Watertank Test

Both systems were tested in a cylindrically shaped watertank (diameter $\approx$ 2.5 m and a depth $\approx$ 2.5 m). The imaging system was attached to two sliding bar tracks which were mounted on the top of the watertank, allowing each camera to take pictures from different view angles. The baseline of imaging system II was detached from the ROV so that it can be calibrated in the same way as the imaging system I. After the calibration was performed in air, the following steps were completed.

1) The calibration frame was placed on the bottom of the watertank and the camera system was mounted on the bar track with each camera and principal optical axis perpendicular to the bottom.
2) Photographs were taken with the housing cover submerged in water.
3) The camera system was shifted along the bar tracks and steps 1) and 2) were repeated to produce image pairs with different view angles.

VI. Experimental Results

A. CCD Imaging System I

A pair of stereo images taken in air were used for the first phase of calibration. Fourteen well-distributed control points (Fig. 7) visible in the stereo pair were used for determining the first set of the calibration parameters. Table I lists the results of the first phase of the calibration which include the interior and exterior orientation parameters $(f, x_p, y_p, s_y, X_o, Y_o, Z_o, \omega, \phi, \kappa)$, the radial lens distortion parameters (K_1, K_2), and the decentering correction parameters (Q_1, Q_2) for both cameras.

The second phase of calibration was to calculate the rest of the imaging system parameters: multilens parameters which define the spherical surface of the cover lenses (a, b, c, and r), those defining the plane surface of the cover (d, e, and g),

TABLE I
Results of the First Phase Calibration (Imaging System I)

Parameter	Left camera	Right camera
f (pixel)	572.99220	590.29455
x_p (pixel)	304.91166	279.57429
y_p (pixel)	231.7966	234.51888
s_y	1.1449	1.1487
X_0(m)	100.6695	100.6010
Y_0(m)	100.6110	100.6013
Z_0(m)	-97.6994	-97.6875
ω (rads)	0.0417	0.0500
ϕ (rads)	-0.2064	-0.1884
κ (rads)	0.0014	-0.0025
$K_1(10^{-2})$	-0.008378	-0.001182
$K_2(10^{-6})$	0.481934	0.337597
$Q_1(10^{-4})$	-0.034693	-0.006720
$Q_2(10^{-4})$	-0.088645	-0.189452

TABLE II
Results of the Second-Phase Calibration (Imaging System I)

Parameter	Left camera	Right camera
a (m)	100.6451	100.7122
b (m)	100.6069	100.5919
c (m)	-98.2102	-98.1710
r (m)	0.0885	0.0909
d	0.0001	0.0001
e	-0.0041	-0.0041
g (m)	98.0779	98.0779
n_2(cover-lens)	1.5999	1.5999
n_3(water)	1.3402	1.3402

TABLE III
Comparison of Calculated and "True" Coordinates in the Object Space (Imaging System I)

Target	Pixel coordinates (pixel)				Difference (m)		
No.	xl	yl	xr	yr	X_c-X_t	Y_c-Y_t	Z_c-Z_t
6	254	461	223	473	0.0085	0.0188	0.0631
9	474	466	446	475	-0.0140	0.0288	0.0473
11	86	205	60	217	0.0073	-0.0008	0.0453
12	79	409	55	423	0.0109	0.0069	0.0498
15	258	423	232	435	-0.0013	0.0050	0.0661
17	448	221	422	232	0.0163	0.0011	-0.0722
19	196	208	168	220	-0.0036	-0.0025	0.0493
20	269	129	240	141	-0.0005	-0.0132	0.0862
21	343	216	315	227	0.0001	-0.0048	0.0201
22	263	286	235	297	-0.005	-0.0044	0.0905
			RMS (m)		0.0087	0.0122	0.0623

TABLE IV
RESULTS OF THE FIRST PHASE CALIBRATION (IMAGING SYSTEM II)

Parameter	Left camera	Estimated Error	Right camera	Estimated Error
f (pixel)	600.56	0.28	596.38	0.28
x_p (pixel)	269.82	0.32	278.74	0.34
y_p (pixel)	230.74	0.88	221.42	0.51
s_y	0.8879	0.70	0.9689	0.84
$X_{0(m)}$	100.3943	0.0014	100.9596	0.0014
$Y_{0(m)}$	100.6710	0.0012	100.5164	0.0016
$Z_{0(m)}$	-97.7869	0.0010	-97.6780	0.0010
ω (rads)	0.0263	0.62	-0.0660	0.50
ϕ (rads)	-0.0144	0.61	-0.0655	0.60
κ (rads)	-0.0156	0.42	0.0013	0.45
$K_1(10^{-2})$	0.0220	0.0124	-0.6315	0.0158
$K_2(10^{-6})$	0.2258	0.0002	0.1886	0.0004
$Q_1(10^{-4})$	0.3968	0.0082	0.3422	0.0102
$Q_2(10^{-4})$	0.2434	0.0002	-0.1715	0.0003

TABLE V
RESULTS OF THE SECOND PHASE CALIBRATION (IMAGING SYSTEM II)

Parameter	Left camera	Estimated Error	Right camera	Estimated Error
d	-0.00000	0.0200	0.00001	0.0224
e	-0.00002	0.0245	-0.00000	0.0256
$g(m)$	97.86935	0.0014	97.89031	0.0014

and the refractive indexes (n_2, n_3). The two CCD cameras were assumed to share the same plane surface and refractive indexes. A stereo image pair taken with the camera system submerged underwater was used. There were nine control points selected for the calibration. The results are illustrated in Table II.

The small differences of attitude parameters of the two cameras revealed in the calibration results (Table I) proved that the optical axes of the two CCD cameras were parallel to within 1.5°. The small values of d and e illustrated that the plane surface of the cover was nearly parallel to the $x - y$ reference plane. The photo-baseline could be easily obtained from the coordinates of two exposure stations and was about 7 cm. A detailed description of mathematical procedures and numerical calculations of the calibration is presented in [1].

With the above parameters calculated by the calibration, 3-D coordinates of points in the object space can be obtained from measured corresponding image coordinates in a stereo pair using the photogrammetric model. To assess the quality of the calibration and the photogrammetric model, a set of control points were selected, which appear in a stereo pair taken underwater and were not used for the calibration. Their image coordinates in pixel units were measured (Table III) and further used to calculate the coordinates (X_c, Y_c, Z_c) in the object space. Since the surveyed coordinates of these control points are of high accuracy (1 mm), they are treated as "true" coordinates (X_t, Y_t, Z_t). Differences between the calculated and "true" coordinates are listed in Table III, which demonstrates the discrepancies in three dimensions for each point. A rms error for each direction is calculated. It is shown that an accuracy around 1.3 cm in the x and y directions in the object space is attainable. But in the direction of the optical axis (z direction), the accuracy is greater than 6 cm, which is much higher than that in the x or y directions.

The base–depth ratio, a ratio between the distance of the cameras B and the depth from the cameras to the measured object $Z°$, is one of the critical factors influencing the final accuracy of the 3-D coordinates of the object. To simplify the error analysis and not to lose the generality, it is assumed that the two cameras are parallel and the error of the parallax of a point is σ_p. The photo scale is $1{:}\,M_{\text{photo}}$. The elevation error of the point derived from the parallax can be determined as [8]

$$\sigma_Z = (Z^o/B) M_{\text{photo}} \sigma_p. \tag{25}$$

σ_p is a constant for a given point and will affect on the accuracy of the depth Z. The depth error σ_Z is inversely proportional to the base–depth ratio B/Z^o. Given a depth Z^o, a wider base B decreases the depth error σ_Z. However, B is usually limited by the physical configuration of the imaging system and to produce an overlapping area for building a stereo model. A base–depth ratio of 2 to 1 will allow relatively homogeneous errors of all three coordinates (X, Y, Z). In mobile systems such as the underwater imaging system, the baseline

is often very small. The depth (Z) errors are consequently greater than lateral errors of X and Y.

Examining the results in Table III for the configuration of this imaging system, the small size of the photo baseline (7 cm) is one of the main factors causing the relatively low measurement accuracy. Because the camera-object distance (depth) is about 2.0 m, the base–depth ratio is so small that a small measurement error in the image space will cause a relatively large displacement in depth direction of the object space.

B. CCD Imaging System II

To overcome the inaccuracies caused by the short baseline in imaging system I and to improve the overall performance, imaging system II was developed with a wider and adjustable baseline and a different configuration. Since the cover lenses have a different form, different parameters are defined to describe the cover lenses. The two cameras have separate housings with flat glass planes. We can image that in Fig. 1, the cover lens is split into two pieces, with each for the left and right camera, respectively. Each cover lens can be described by a flat glass plane with a thickness of r. Both faces of the glass plane are parallel and depicted by $dX + eY$ and $Z + g = 0$. Thus, cover lens parameters are (d, e, g, r). The remaining parameters are same as those in imaging system I.

Four parameters can be measured precisely without the photogrammetric adjustment: $r = 16$ mm, $n_1(air) = 1.00$, $n_2(glass) = 1.65$, and $n_3(water) = 1.34$. Fifteen control points appearing in an "in air" image pair were applied to perform the first phase of the calibration. Table IV lists the parameters and corresponding errors estimated. These parameters were treated as the knowns in the second phase calibration. Using fifteen control points measured from an "underwater" image pair, three remaining parameters were estimated (Table V). The parameters calibrated in both phases were then used to compute 3-D coordinates in the object space from measured image coordinates of any point visible in the stereo pair. In Table VI, the image coordinates and the corresponding differences between the computed and "true" coordinates in the object space of eleven check points are illustrated.

Comparing with the experiment result of imaging system I, it is obvious that the overall accuracies of the 3-D coordinates in X, Y, and Z directions are greatly improved. This is mainly due to the increase of the baseline width from 7 to 40 cm, with the depth remaining about the same. The new base–depth ratio is about 1/5.

TABLE VI
COMPARISON OF CALCULATED AND "TRUE" COORDINATES IN THE OBJECT SPACE (IMAGING SYSTEM II)

Target	Pixel coordinates *(pixel)*				Difference *(m)*		
No.	*xl*	*yl*	*xr*	*yr*	X_c-X_t	Y_c-Y_t	Z_c-Z_t
1	180	32	66	26	0.0035	0.0024	-0.0012
2	175	209	57	203	0.0073	-0.0007	0.0028
4	374	32	256	23	0.0044	0.0003	0.0013
10	202	64	103	58	-0.0112	-0.0101	0.0013
18	521	363	426	362	-0.0057	-0.0030	-0.0016
9	563	390	450	389	0.0009	-0.0055	0.0105
16	522	68	428	59	0.0028	0.0085	0.0018
6	370	393	249	389	0.0028	-0.0112	0.0025
24	476	391	358	390	0.0073	-0.0031	-0.0125
5	374	210	254	204	-0.058	-0.0077	0.0075
19	298	214	196	207	-0.0069	-0.0063	0.0104
			RMS *(m)*		0.0060	0.0063	0.0065

VII. CONCLUSION

A photogrammetric model for digital underwater video imagery has been researched. With this model, quantitative analysis of underwater images can be carried out, e.g., to locate positions, calculate sizes, and measure shapes of objects from stereo images. In addition, a PC-based digital underwater photogrammetric prototype system has been developed to implement the underwater photogrammetric model. From the research results, the following major conclusions can be drawn.

- The 3-D optical ray tracing technique is an effective way to construct a rigorous photogrammetric model for the imaging systems in a multimedia and multilens involvement.
- The calibration procedure with two independent phases has been proven to be efficient in simplifying the computation and improving the calibration accuracy.
- With the current imaging system configuration and the photogrammetric model, an accuracy of 0.8 cm along the x and y direction and 1.2 cm along the z direction for objects located about 2-3 m from the camera system in the object space is attainable.
- The base–depth ratio is critical in determining the accuracy of the system, especially along the optical axis direction.

For the further research and development of this system, the configuration of the imaging system should be optimized. Multiple images taken from different exposure stations might be used simultaneously for the calibration in order to achieve more robust results. In addition, the design of the calibration frame could be modified from a rectangular-shaped frame to a trapezoidal one. This guarantees that additional control targets on the calibration frame will not block each other when images are taken from different viewing angles. Variation of image distortions with object space distances should also be examined. Finally, image matching techniques [29], [30] should be employed to automate the measuring procedure and support other quantitative analysis functions.

ACKNOWLEDGMENT

The helpful comments from the reviewers are appreciated.

REFERENCES

[1] H. Li, "Quantitative analysis of underwater stereo video images," masters thesis, Dept. of Geomatics Eng., Univ. of Calgary, Calgary, Alberta, Canada.

[2] P. R. Zwart and D. Tay, "Measuring the shape of fishnets—An application of three media close range photogrammetry," in *Symp. Application of Close Range Photogrammetry*, University of Melbourne, Australia, 1987.
[3] R. A. Badwin, "An underwater photogrammetric measurement system for structure inspection," *Int. Arch. Photogrammetry*, vol. 25, no. A5, pp. 49–58, 1984.
[4] F. M. Caimi, D. C. Smith, and D. M. Kocak, "Undersea 3-D imaging and mapping for inspection and research," *Adv. Imaging*, vol. 7, pp. 32–36, July 1992.
[5] J. Pollio, "Underwater mapping with photography and sonar," *Photogrammetric Eng.*, vol. 37, no. 9, pp. 955–968, 1971.
[6] H.-G. Maas, "Robust automatic surface reconstruction with structured light," *Int. Arch. Photogrammetry Remote Sensing*, vol. XXIX, pt. B5, pp. 709–713, 1992.
[7] R. F. Tusting and D. L. Davis, "Laser systems and structured illumination for quantitative undersea imaging," *MTS J.*, vol. 26, no. 4, pp. 5–12, 1992.
[8] P. R. Wolf, *Elements of Photogrammetry.* New York: McGraw-Hill, 1983.
[9] F. H. Moffitt and E. M. Mikhail, *Photogrammetry.* New York: Harper & Row, 1980.
[10] C. C. Slama, C. Theurer and S. W. Henriksen, Eds., *Manual of Photogrammetry*. Falls Church, VA: Amer. Soc. Photogrammetry, 1980.
[11] H. Takasaki, "Simultaneous all-around measurement of a living body by Moirè topography," *Photogrammetric Eng.*, vol. 40, no. 12, 1974.
[12] J. Pollio, "Photogrammetric applications to undersea tasks," *J. Soc. Motion Picture Television Eng.*, vol. 78, no. 12, pp. 152–157, 1969.
[13] A. K. I. Torlegard and T. L. Lundalv, "Undersea analytical systems," *Photogrammetric Eng.*, vol. 40, no. 3, pp. 287–293, 1974.
[14] N. Welsh, I. K. Leadbetter, O. W. Cheffins, and H. M. Hall, "Photogrammetric procedures for a North Sea oil rig leg repair," *Int. Arch. Photogrammetry*, vol. 23, no. B5, pp. 474–483, 1980.
[15] R. A. Badwin and I. Newton, "A proposed system for underwater photogrammetry from a manned submersible camera platform," *Int. Arch. Photogrammetry*, vol. 24, no. 5, pp. 39–52, 1982.
[16] E. Kristof, A. Chandler, and W. Hamner, "3-D as an underwater tool," in *IEEE Proc. Oceans 88*, New York, pp. 713–718.
[17] J. D. Leatherdale and D. J. Turner, "Underwater photogrammetry in the North Sea," *Photogrammetric Rec.*, vol. 11, no. 62, pp. 161–167, 1983.
[18] ———, "Operational experience in underwater photogrammetry," *ISPRS J. Photogrammetry Remote Sensing*, vol. 46, pp. 104–112, 1993.
[19] J. G. Fryer, "Underwater 35mm photogrammetric applications in Australia," *Int. Arch. Photogrammetry*, vol. 24, no. 5, pp. 167–174, 1982.
[20] L. P. Adams, "Underwater analytical photogrammetry using nonmetric cameras," *Int. Arch. Photogrammetry*, vol. 24, no. 5, pp. 12–22, 1982.
[21] J. Hoehle, "Reconstruction of the underwater object," *Photogrammetric Eng.*, vol. 39, no. 9, pp. 949–954, 1971.
[22] A. Okamoto, "Orientation problem of two-media photographs with curved boundary surfaces," *Photogrammetric Eng. Remote Sensing*, vol. 50, no. 3, pp. 303–316, 1984.
[23] A. W. Gruen, "Digital photogrammetric processing system: Current status and prospects," *Photogrammetric Eng. Remote Sensing*, vol. 55, no. 5, pp. 581–586, 1989.
[24] C. Heipke, "State-of-the-art of digital photogrammetric workstations for topographic applications," *Photogrammetric Eng. Remote Sensing*, vol. 61, no. 1, pp. 49–56, 1995.
[25] D. J. Turner and D. J. Yule, "A digital noncontact measurement system," *Photogrammetric Rec.*, vol. 14, no. 82, pp. 583–594, 1993.
[26] D. C. Brown, "Evolution and future of analytical photogrammetry," Rep. no. 250, The Changing World of Geodetic Science, Dept. of Geodetic Science, The Ohio State Univ., pp. 360–410, 1977.
[27] R. Laurini and D. Thompson, *Fundamentals of Spatial Information Systems.* New York: Academic, 1992.
[28] Miller and Lin, *The COGO Book.* Tampa, FL: CLM/Systems, 1990.
[29] R. Li, "Building Octree representations of 3-D objects in CAD/CAM by digital image matching techniques," *Photogrammetric Eng. Remote Sensing*, vol. 58, no. 12, pp. 1685–1691, 1992.
[30] L. Qian, Y. Xin, R. Li, and M. A. Chapman, "Reconstruction of geometric elements in GIS databases using GPS/INS controlled CCD images," in *Proc. GIS'94*, Vancouver, BC, Canada, pp. 395–398.

Rongxing Li received the B.Sc. and M.S. degrees in surveying and mapping from Tongji University, Shanghai, China, and the Doctor of Engineering degree in photogrammetry and remote sensing from the Technical University of Berlin, Berlin, Germany.

Before joining The Ohio State University, Columbus, in 1996 as an Associate Professor in the Department of Civil and Environmental Engineering and Geodetic Science, he was Associate Professor in the Department of Geomatics Engineering at the University of Calgary, Calgary, Canada. From 1990 to 1992, he was an Assistant Researcher at the Pacific Mapping Center of the University of Hawaii. His current research interests include digital photogrammetry and vision, real-time and mobile mappings, 3-D GIS, marine and coastal GIS, and virtual reality.

Haihao Li received the B.Sc. degree in microelectronics from Beijing University, Beijing, China, and the M.Sc. degree in photogrammetry and remote sensing from the University of Calgary, Calgary, Canada.

During his studies at the University of Calgary,, he was in involved in research on digital photogrammetry. He is presently a Systems Engineer with MCI Systemhouse.

Weihong Zou, photograph and biography not available at the time of publication.

Robert G. Smith, photograph and biography not available at the time of publication.

Terry A. Curran, photograph and biography not available at the time of publication.